Detection of Leukocytes in Intravital Video Microscopy Based on the Analysis of Hessian Matrix Eigenvalues

Bruno C. Gregório da Silva, Ricardo J. Ferrari
Department of Computer Science
Federal University of São Carlos
São Carlos, SP, Brazil
Email: {bruno.silva, rferrari}@dc.ufscar.br

Juliana Carvalho-Tavares
Department of Physiology and Biophysics
Federal University of Minas Gerais
Belo Horizonte, MG, Brazil
Email: julianat@icb.ufmg.br

***Abstract*—Detection of rolling and adhered leukocytes in intravital microscopy image sequences is an important task in studies of leukocyte-endothelial interactions in the microcirculation of living small animals under different inflammatory conditions. This procedure is usually performed by visual assessment of the image sequences. However, despite being tedious and time consuming, this procedure is prone to the inter- and intra-observer variability. In this work, we developed an automated computer system for the detection of leukocytes in intravital video microscopy. First, the video frames were processed by the bilateral filter to reduce noise while preserving sharp edges. Then, a demons-based image registration technique was applied to minimize animal motion. Finally, the detection of leukocytes was performed by local analysis of Hessian matrix eigenvalues. Quantitative and qualitative evaluation of the proposed method were conducted by using 220 video frames obtained from an experimental study performed on the brain microvasculature of mice. The proposed method was compared with the template matching technique using precision, recall and F1-Score measures. For the Hessian-based method, the results of precision, recall and F1-Score were, respectively, equal to 0.81, 0.86, and 0.83. For direct comparison, the results obtained for the template matching technique were 0.86, 0.73 and 0.79.**

***Keywords*—detection of leukocytes; intravital video microscopy; temporal image registration**

I. INTRODUCTION

Analysis of rolling and adhered leukocytes is an important task to study the mechanisms underlying leukocyte-endothelial interactions in the microcirculation of living small animals under different inflammatory conditions [1]. Such studies may have important implications on the design of new therapeutic strategies to fight inflammation. Intravital microscopy is currently the gold standard technique for the study of the in *vivo* microcirculation because it allows direct observation of leukocyte movement in microvessels of small animals under both normal and pathological conditions [2]. In laboratory experiments, the microscopic images are usually recorded on a digital media during the experiment for further visual analysis. However, visual assessment is a time-consuming, tedious, and an error-prone task. Automatic dynamic analysis of the behavior of rolling and adhered leukocytes is a difficult task in computer vision due to severe image noise and clutter, high variability in contrast between cells and background (due to differences in focal depth) and the unavoidable presence of motion blur in the images, caused by heart beat and respiratory movements of the animal.

A number of methods have been described in the literature for the detection and tracking of leukocytes in intravital video microscopy (IVM). Sato *et al.* [3] have detected only leukocytes rolling along the vessel walls. For that, they have processed the spatial path parallel and near to the vessel contour in the images. Bandpass filtering operation was used to generate spatio-temporal images in which leukocyte traces are enhanced while other components are suppressed.

Acton *et al.* [4] have also proposed a method to automatically track leukocytes in IVM. Their tracker first performs registration of each pair of consecutive frames. Then, the authors time-average the registered frames to obtain an estimate of the background and proceed by subtracting the background from all frames, leaving only the moving objects in the foreground. An open-close morphological filter was used to eliminate both bright and dark features that are smaller than a structuring element. Finally, adaptive template matching and Kalman filter were applied for cell tracking. By using over 2500 observations of leukocyte positions, the authors demonstrated that automated tracking of rolling leukocytes *in vivo* can be achieved.

Ray *et al.* [5] proposed an active contour model for tracking leukocytes. In their work, model adaptation was constrained by using shape and size of cells. Detection of leukocytes was then converted into a minimization problem, where the energy functional was composed of three energy components (internal, external and constraint). Despite the good results, the method can track only one leukocyte at a time and it is based on user initialization of the leukocyte center positions, which may not be feasible for analysis of hundreds of cells in an image sequence. Furthermore, their proposed model is sensitive to the proximity of the cell to the vessel wall. Modifications of these previous methods by incorporating the Gradient Vector Flow (GVF) technique [6] and an extension of the GVF for image sequences [7] were published by the same research group. Level set was also used to detect and track multiple cells in IVM by searching for candidate cells in the image level lines (boundaries of connected components within level sets) [8]. The authors also proposed stochastic methods for the detection and tracking of leukocytes [9], [10].

In this work we present a new method for the detection of leukocytes in intravital image sequences that presents two main contributions: first, we have developed a video motion stabilization method that uses two stages of image registration (affine and deformable) embedded in a multiscale framework to allows for a high-accurate alignment of the video frames; second, we propose a new method for the detection of leukocytes that is based on the eigenvalue analysis of Hessian matrix. The paper is organized as follows: Section II describes the methodology and the image dataset used in this work, followed by results and discussions in Section III and conclusions in Section IV.

II. METHODOLOGY

The detection of leukocytes in intravital microscopy image sequences is a challenge problem due to the high noise level present in the images, the wide ranging appearance of leukocytes (in intensity and shape), and mainly to motion blur and artifacts caused by respiratory and cardiac motion. In this work all images were preprocessed using an automated pipeline, as indicated in Figure 1. In the first stage, all frames strongly affected by the animal movement were detected and removed by a technique previously developed for this purpose [11]. Although image restoration techniques can be used to recover the motion-blurred frames, in this work we have only extracted them from further analysis. In the next stage, bilateral filtering [12], which has the ability to reduce noise without introducing noticeable blurring, was applied to improve image quality. The parameters of the filter ($d = 9$, $\sigma_r = 10$ and $\sigma_d = 10$ corresponding, respectively, to the diameter of filter neighborhood and to the range and spatial parameters of Gaussian kernels) were experimentally adjusted to provide the best trade-off between noise reduction and low blurring effect. In order to diminish the photobleaching effect [13], commonly observed in fluorescence microscopy, and to improve our frame-to-frame image registration method (described in details in Section II-A), the histogram matching technique proposed in [14] was applied to each pair of consecutive frames in the video. After registration, the vessel region was extracted by assessing the temporal variance of each pixel, as proposed in [3]. The rationale in this case is that the gray level of each pixel in a vessel region, where blood cells are flowing continuously, will greatly vary within frames while the gray level in other regions will be almost constant — i.e., the gray level variance tends to be large in the vessel region and small in other regions. After that, a binary vessel image was created and used in further analysis to reduce the number of false-positive cells automatically detected in the images. Finally, all frames were processed for the detection of the leukocytes, as described in Section II-B.

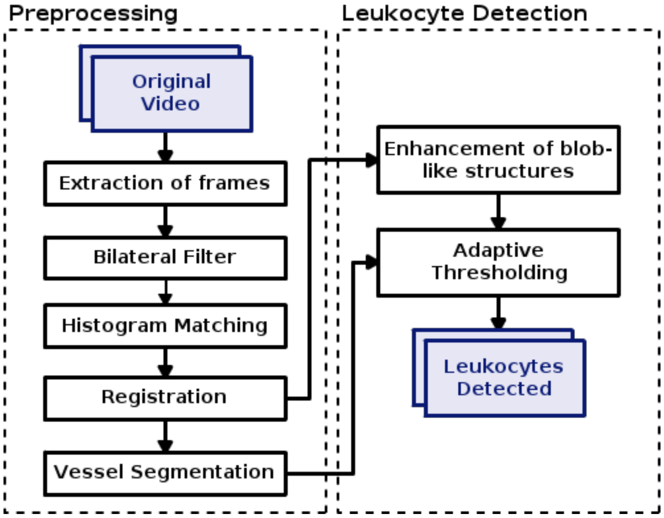

Fig. 1. Flow diagram of the proposed method to detect leukocytes in intravital microscopy image sequences.

A. Temporal image registration

The temporal image registration framework developed in this work to correct for small specimen movements is comprised of four modules: metric, optimizer, interpolator and transformation. The method, as shown in Figure 2, consists of finding a transformation $T(p)$ to correct the misalignment between consecutive pair of frames (images) in the video. The set of parameters p of the transformation T is obtained in an iterative manner by mapping all pixels from the moving frame $M(x, y)$ to their corresponding pixels in the fixed frame $F(x, y)$ so that the similarity metric $S(p|F, M, T)$ is minimized.

1) Metric: The metric chosen in this work was the mutual information (MI) [15], which measures the statistical dependency between two data sets (fixed and moving images) by taking into account the amount of information that one random variable has over another. MI is defined in terms of entropy in the following way [15]:

$$\begin{aligned} S(p|F, M, T) &= MI\,(F, T) \\ &= H\,(F) + H\,(M|T) - H\,(F, M|T)\,, \end{aligned} \tag{1}$$

where $H\,(\cdot)$ is the entropy of a random variable (in this case, images F or M), which can be calculated from the marginal probability (normalized intensity histogram), $P\,(\cdot)$, of the images as:

$$H\,(F) = -\sum_{m \in F} P\,(m) \log P\,(m)\,, \tag{2}$$

$$H\,(M|T) = -\sum_{n \in M} P\,(n|T) \log P\,(n|T)\,. \tag{3}$$

In Equations (2) and (3), m and n represent, respectively, pixel intensities in the images F and M. The joint entropy of images F and M, which is the last term in Equation (1),

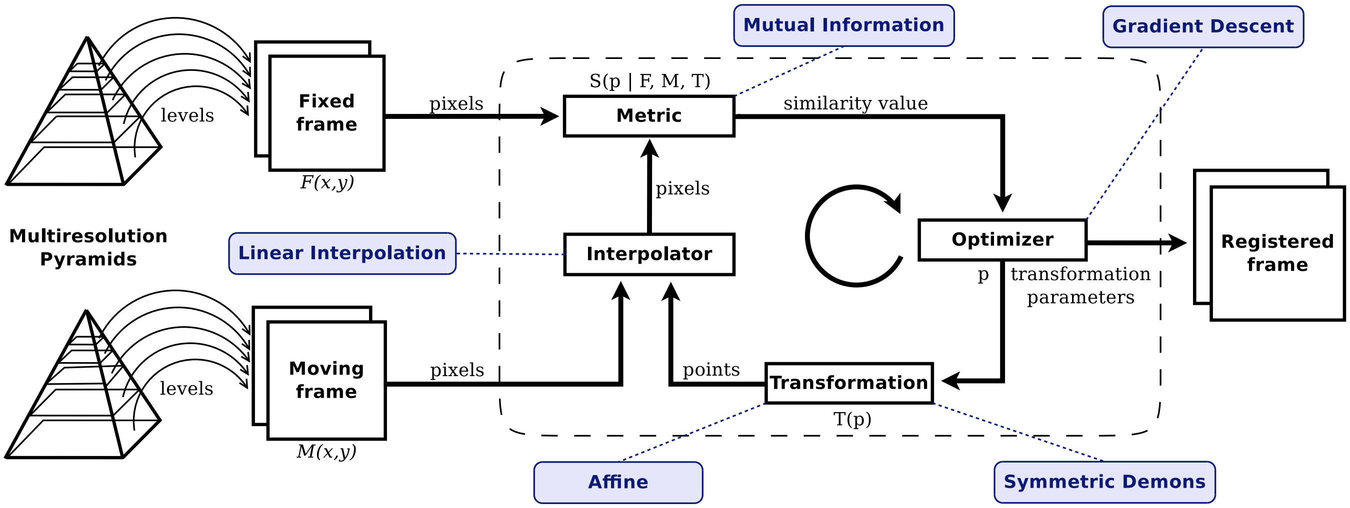

Fig. 2. Temporal image registration framework developed to stabilize video motion due to small animal movements.

is calculated from their joint probability distribution (joint normalized intensity histogram), $P(m, n|T)$, as:

$$H\left(F, M|T\right) = -\sum_{m\in F, n\in M} P\left(m, n\right) \log P\left(m, n|T\right). \quad (4)$$

2) Optimizer: An optimizer based on the gradient descent method [16] was used to search for the best set of parameters p that minimizes the similarity function S between images F and M. The method uses a multiresolution Gaussian pyramid approach in which the levels contain images with different resolutions, as illustrated in Figure 2. The parameters estimation starts with the lowest resolution images ($(692 \times 520) \div 2^n$, where $n = 4$ is the number of decomposition levels used in this work) in the top level of the pyramids, and the parameters estimated at this level are used as an initial start to the algorithm on the next lower level of the pyramids (higher resolution images). This procedure is then repeated until the pyramid bases (full resolution images) are reached. This approach results in a reduction of processing time of the algorithm as well as in an increase in the method's stability, since the coarse details from the top levels of the pyramids increase the chance of the gradient descent method to converge to a point of global minimum, providing, therefore, good parameters estimation in each iteration.

The choice of using the gradient-descent algorithm as an optimizer in our registration framework was made because it is a low computational complexity technique, which is an important feature when processing very large amounts of data. Also, as mentioned previously, the optimization of the parameters is performed using a multiresolution framework, which minimizes the chances of the gradient-descent algorithm getting trapped in a local minimum and increases the convergence speed.

3) Interpolator: Similarly to the optimizer, a linear interpolator was used in our image registration framework because of its low computational complexity with respect to the number of image pixels. This module is necessary because the mapping of the points from one image into another is performed in the physical coordinate system and, therefore, an interpolator is required to put these points back in their corresponding places in the image pixel grid.

4) Transformation: Mathematically, geometrical transformations represent mappings of points from a space X of one view (moving image) to a space Y of a second view (fixed image). As indicated in Figure 2, our proposed method uses two types of geometrical transformation to correct for undesirable frames misalignment caused by the animal movements. First, an affine transformation T, which represents a linear combination of rotations, translations, scaling and shearing operations, was applied to each position $\boldsymbol{x}$ of the moving image (herein, a point in X is represented by the column vector $\boldsymbol{x}$) to produces a transformed point $\boldsymbol{x}'$,

$$\boldsymbol{x}' = T(\boldsymbol{x}). \quad (5)$$

This transformation results in a coarse alignment between the moving and fixed images.

After the affine registration, the deformable transformation technique proposed in [17] was applied to the moving image to refine the previous computed alignment. A deformable transformation consists of finding a mapping of an image $M(\boldsymbol{x})$ to an image $F(\boldsymbol{x})$ using a deformation field $u(\boldsymbol{x})$ [18]. The deformation is defined in the physical image space and provides the positional difference between two given images. In this way, if a feature defined in $F(\boldsymbol{x})$ has its equivalent in $M(\boldsymbol{y})$, the deformation field u in $\boldsymbol{x}$ is computed as

$$u(\boldsymbol{x}) = \boldsymbol{y} - \boldsymbol{x}, \quad (6)$$

and, therefore, it can be applied to deform an image M into an image F by

$$M_{deformed} = M(\boldsymbol{x} + u(\boldsymbol{x})). \quad (7)$$

The idea of the deformable transformation technique [17] to compute the deformation field is that a regular grid of forces deforms an image by pushing the contours in the normal directions. The orientation and magnitude of the displacement vectors are derived from the instantaneous optical flow equation [19]. In this case, the conservation of gray level intensity of the moving points is assumed to be constant, i.e., $I(\boldsymbol{x}(t), t) = const$, with $\boldsymbol{x}(t)$ representing the coordinates of the point at time t.

In our case, two consecutive pair of frames (the fixed frame denoted by $F(\boldsymbol{x})$ and the moving frame $M(\boldsymbol{x})$) are compared to allow the computation of displacement vector $u(\boldsymbol{x})$ that let $M(\boldsymbol{x})$ closer to $F(\boldsymbol{x})$. Then, by considering that $F(\boldsymbol{x})$ and $M(\boldsymbol{x})$ are separated by one time unit, ${}^{\partial I}/_{\partial t} = M(\boldsymbol{x}) - F(\boldsymbol{x})$ and $u(\boldsymbol{x}) = {}^{d\boldsymbol{x}}/_{dt}$ is the instantaneous velocity of $F(\boldsymbol{x})$ to $M(\boldsymbol{x})$, thus

$$u(\boldsymbol{x}) \cdot \nabla F(\boldsymbol{x}) = -\left(M(\boldsymbol{x}) - F(\boldsymbol{x})\right). \tag{8}$$

In this case, $u(\boldsymbol{x})$ is considered to be velocity because the images are two successive time frames, i.e., $u(\boldsymbol{x})$ is the displacement during the time interval between the two image frames [17]. It is well known in optical flow literature that Equation 8 is not sufficient to define the velocity $u(\boldsymbol{x})$ locally and, in this case, it is usually determined using some form of regularization. For registration, the projection of the vector on the direction of the intensity gradient is used as:

$$u(\boldsymbol{x}) = -\frac{\left(M(\boldsymbol{x}) - F(\boldsymbol{x})\right) \nabla F(\boldsymbol{x})}{\|\nabla F\|^2 + {}^{(M(\boldsymbol{x})-F(\boldsymbol{x}))^2}/_K}, \tag{9}$$

where K is a normalization factor that accounts for the units imbalance between intensities and gradients. This factor is computed as the mean squared value of the pixel spacings. Inclusion of K makes the force computation to be invariant to pixel scaling in the images. In order to provide a level of symmetry in the force calculation, a variation of the equation 9 was used. In this case, the gradient of the deformed moving image is also involved, so that

$$u(\boldsymbol{x}) = -\frac{2 \cdot \left(M(\boldsymbol{x}) - F(\boldsymbol{x})\right) \left(\nabla F(\boldsymbol{x}) + \nabla M(\boldsymbol{x})\right)}{\|\nabla F + \nabla M\|^2 + {}^{(M(\boldsymbol{x})-F(\boldsymbol{x}))^2}/_K}. \tag{10}$$

An elastic-like behavior, smoothing the deformation field with a Gaussian filter between iterations, was included into the implemented algorithm in order to make it realer.

B. Detection of leukocytes

Although leukocytes slightly change from circular to an oval shape before transmigrating through the endothelium, in this work our assumption is that these cells can be visualized as blob-like structures in IVM. Therefore, our proposed method for the automatic detection of leukocytes is based on a salient blob detector approach that uses information of Hessian matrix eigenvalues for the representation of local geometric structures [20] (blob-like structures, in our case) in an image.

Since microscopic images are two-dimensional projections of three-dimensional structures (microvessels and cells), leukocytes may be positioned above and below the microscope focal plane and, therefore, their size appearance may be distorted, showing cells in a different range of scales. For this reason, our proposed method was developed based on the analysis of local structures in a multiscale framework [20]. The initial idea of our approach is to generate a family of smoothed images $I(x, y; \sigma)$, computed by convolving the original image $I_0(x, y)$ with Gaussian kernels $G(x, y; \sigma)$ of different standard deviation (σ) values, as

$$I(x, y; \sigma) = I_0(x, y) * G(x, y; \sigma), \tag{11}$$

where

$$G(x, y; \sigma) = \frac{1}{\sigma\sqrt{2\pi}} \exp\left(-\frac{1}{2}\left(\frac{x+y}{\sigma}\right)^2\right), \tag{12}$$

and use a strategy to proper select the local scale parameter to build the Hessian matrix. For that, the response function $R(x, y; \sigma)$, computed as

$$\begin{aligned} R(x, y; \sigma) &= \frac{\partial^{m+n} I(x, y; \sigma)}{\partial x^m \partial y^n} && (13) \\ &= I_0(x, y) * \frac{\partial^{m+n} G(x, y; \sigma)}{\partial x^m \partial y^n}, && (14) \end{aligned}$$

where m and n are orders of derivatives, was used. The local scale was defined as the value of σ (over a range of values) corresponding to the maximum value of function $R(x, y; \sigma)$ for each pixel, which indicates the proper Gaussian scale probe (Gaussian observation kernel) with the width value corresponding to object feature size. Because of the amplitude of Gaussian derivative operators in (14) tends to decrease with increasing scale (due to the fact that with increasing scale, the response is increasingly smoothed), the so-called γ-parameterized normalized derivatives [21],

$$\frac{\partial^{m+n}}{\partial u^m \partial v^n} = \sigma^{(m+n)\gamma} \frac{\partial^{m+n}}{\partial x^m \partial y^n}, \tag{15}$$

with $\gamma = 1.25$, was used in this work to overcome this problem. The choice of $\gamma = 1.25$ was experimentally determined to work well on a variety of intensity structure profiles [22].

Based on the intensity responses of the γ-parameterized normalized derivative filters, a local measure of image structure is devised from the analysis of Hessian matrix eigenvalues of image intensity. For a given scale σ, the Hessian matrix $H_\sigma(I)$ of an image I is a square and symmetric matrix composed of second-order partial derivatives,

$$H_\sigma(I) = \begin{bmatrix} I_{\sigma_{xx}} & I_{\sigma_{xy}} \\ I_{\sigma_{yx}} & I_{\sigma_{yy}} \end{bmatrix}, \tag{16}$$

where

$$I_{\sigma_{xx}} = I_0(x, y) * \left(\sigma^{2\gamma} \frac{\partial^2}{\partial x^2} G(x, y; \sigma)\right), \tag{17}$$

$$I_{\sigma_{yy}} = I_0(x, y) * \left(\sigma^{2\gamma} \frac{\partial^2}{\partial y^2} G(x, y; \sigma)\right), \text{ and} \tag{18}$$

$$I_{\sigma_{xy}} = I_{\sigma_{yx}} = I_0(x, y) * \left(\sigma^{2\gamma} \frac{\partial^2}{\partial x \partial y} G(x, y; \sigma)\right). \tag{19}$$

Mutual magnitude of eigenvalues from Hessian matrix is an indicative of the underlying object shape. Under the assumption that eigenvalues are sorted in order of increasing absolute value ($|\lambda_1| \leq |\lambda_2|$), the relations that must hold between the Hessian matrix eigenvalues for the detection of different structures are summarized in Table I.

TABLE I
POSSIBLE PATTERNS IN 2D, DEPENDING ON THE VALUE OF THE EIGENVALUES λ_k (H=HIGH, L=LOW, N=NOISY, USUALLY SMALL, +/- INDICATE THE SIGN OF THE EIGENVALUE) [23]. THE EIGENVALUES ARE ORDERED: $|\lambda_1| \leq |\lambda_2|$.

$\boldsymbol{\lambda_1}$	$\boldsymbol{\lambda_2}$	**orientation pattern**
N	N	noisy, no preferred direction
L	H-	tubular structure (bright)
L	H+	tubular structure (dark)
H-	H-	blob-like structure (bright)
H+	H+	blob-like structure (dark)

In the intravital microscopy images used in this work, leukocytes emerge as bright blob-like structures embedded in a dark background. Because of the images are affected by noise, we need to address the problem of effective enhance the cells contrast without increasing the image noise level.

By treating the problem of leukocyte detection as a Hessian eigenvalue analysis, we can easily incorporate the cell shape information into the solution. In this way, prior information can be used as a consistency check to discard structures present in the dataset with different polarity than the one sought. Isotropic structures, for instance, are associated to eigenvalues having a similar non-zero magnitude. Accordingly, we shall look for structures whose λ_1 and λ_2 are both, simultaneously, high and negative. By taking this into consideration, a blobness measure function $B_\sigma(\boldsymbol{\lambda})$, defined as

$$B_\sigma(\boldsymbol{\lambda}) = \begin{cases} \left(1-\exp\left(-\frac{R_A^2}{2\alpha^2}\right)\right)\times & \\ \left(1-\exp\left(-\frac{S^2}{2\beta^2}\right)\right) & if\, \lambda_1 < 0 \text{ and } \lambda_2 < 0, \\ 0 & \text{otherwise,} \end{cases} \tag{20}$$

was created by using the ratio and magnitude strength of the eigenvalues and used to enhance blob-like structures representing the leukocytes in the images. In Equation (20), $R_A = |\lambda_1|/|\lambda_2|$ helps distinguishing between plate-like and line-like patterns. In addition, the measure $S = \sqrt{\lambda_1^2 + \lambda_2^2}$ helps to reduce the influence of background noisy pixels in the blobness measure function, since noisy pixels present low eigenvalues and, therefore, the second term in Equation (20) will considerably reduce the blobness value. Parameters α and β can be adjusted to control the sensitivity of the filter components and, in this work, they were set, respectively, to 0.5 and one tenth of the maximum value of the Laplacian of the image, as suggested in [20]. The σ footer in B_σ indicates that the blobness measure is computed on a smoothed version of the image and, therefore, it is representative of the variations of image intensity at the spatial scale σ. The function was evaluated at range of spatial scales (σ), varying between 2 and 3. This range was based on the size of the observed leukocytes in the images. The maximum response at every pixel was taken as

$$B(\boldsymbol{\lambda}) = \max_{\sigma \in [\sigma_{min}, \sigma_{max}]} B_\sigma(\boldsymbol{\lambda}). \tag{21}$$

As result, we have an image sequence containing all possible blob-like structures detected by the algorithm. As mentioned previously, as the leukocytes may be positioned above and below the microscope focal plane, their apparent size and, specially their contrast, can significantly change in the images. For this reason, the multiscale blob detector will produce real-valued responses. Therefore, to improve cells detection, an adaptive thresholding technique was applied to the blob detector output image. In this case, the local threshold value was calculated as a weighted sum (cross-correlation with a Gaussian window) of an $M \times M$ neighborhood of position (x, y) in the image. The default standard deviation of the Gaussian window is defined by the specified neighborhood size M. In this approach we set $M = 17$ by considering the radius of the largest leukocyte.

After binarization by the local threshold technique, pixels corresponding to candidates cells were extracted from the original frames. Finally, with these pixel values, we refined the output images choosing only the regions that have an average value larger than a threshold. This process was conducted to prune low blob responses, probably due to noisy pixels. This threshold value was varied from 1 to 255 at step of 1 and the results of this stage are analyzed in Section (III).

C. Intravital microscopy dataset

For this work, female C57BL/6 mice between 9 and 10 weeks of age were obtained from Animal Care Facilities of the Federal University of Minas Gerais (UFMG, Brazil). The Animal Ethics Committee of UFMG approved all experimental procedures used in this study. Intravital microscopy was performed on the mouse brain microvasculature as previously described [24]. Each mouse was anesthetized using an intraperitoneal injection of ketamine/xylazine and its tail vein was cannulated for the i.v. administration of 200 μL of rhodamine 6G dye (0.5 mg/mL). The animal was restrained in a stereotactic rodent head holder and craniotomy was performed using a high-speed drill. The dura matter was removed to expose the underlying pial vasculature. After the surgeries, each animal was transferred to the microscope stage and was maintained at 37°C using a heating pad (Fine Science Tools Inc., Canada). The exposed brain window was superfused continuously with artificial cerebrospinal fluid buffer at 37°C. To assess the leukocyte-endothelial interactions, the fluorescent leukocytes were visualized under a Zeiss Imager M.2 (x20 long-distance objective lens; Göttingen, Germany) equipped with a fluorescent light source (epi-illumination at 510–560 nm, using a 590 nm emission filter). A video camera (Optronics) was mounted on the microscope in order to record images with a sampling rate of 16 frames/s, 8 bits depth and spatial resolution of 1.89 pixels/μm with a matrix size of 692×520 pixels. Microvessels were analyzed in sections

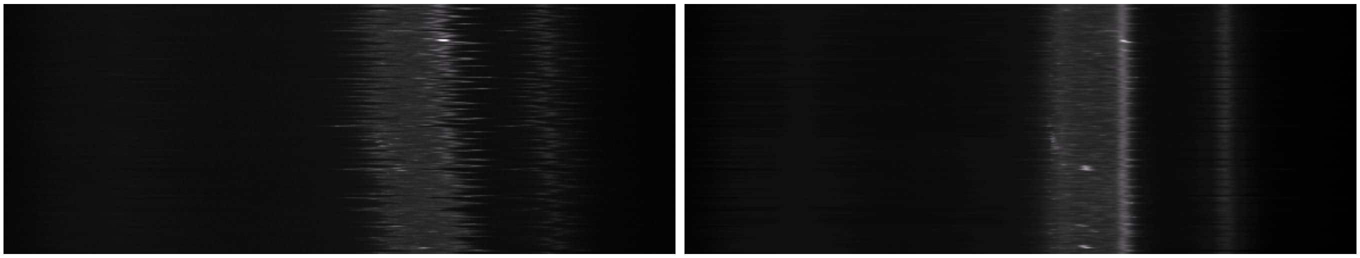

(a) (b)

Fig. 3. Line projection results. (a) Line projection image before and (b) after registration technique.

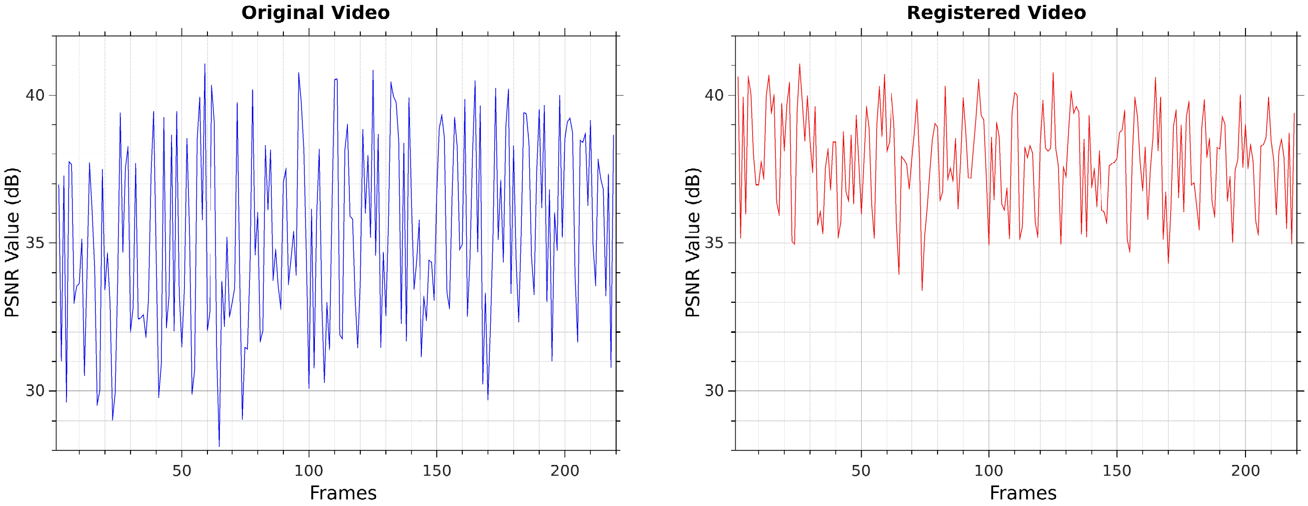

(a) (b)

Fig. 4. PSNR metric processed over all the residual images from all consecutive video frames. (a) PSNR values before and (b) after registration.

of 100 μm in length, and the diameters of the vessels ranged from 40 to 115μm in the brain.

D. Ground-truth image dataset

A total of 220 frames of an IVM containing 5851 leukocytes (obtained from the experiment described in Section II-C) was used to quantitatively assess the results of the proposed method. For this purpose, all leukocyte centroids were manually annotated frame-by-frame with help of a computer program. All annotations, containing an average of 26.6 leukocytes per frame, were checked by an expert biologist (JCT), co-author of this paper.

III. RESULTS AND DISCUSSIONS

The temporal image registration algorithm, as described in Section II-A, was visually assessed by using the line projection technique. This technique works by stacking the central line of each video frame to create a new image, where the intensity profile of each frame line is arranged horizontally while the time sequence is assessed vertically. The result of applying this technique to our image dataset is shown in Figure 3.

By comparing both projections in Figure 3, a noticeable sawtooth pattern can be seen in (a). This pattern indicates a strong misalignment of the frames throughout the image sequence before registration. On the other hand, in image (b) the sawtooth pattern is less noticeable, indicating more continuous lines and consequently a greater alignment of the frames after the registration process.

Quantitative analysis of the temporal image registration algorithm was conducted by calculating the peak signal-to-noise ratio (PSNR) metric for residual images resulting from subtraction of consecutive pair of frames, before and after registration. This measure defines the ratio between the maximum possible power of a signal and the power of corrupting noise that affects the fidelity of its representation on the video frames. In case of good alignment, the residue will be small and PSNR value (dB) will be large. Otherwise, if residue is large, then PSNR value will be small. PSNR values calculated, before and after registration, for all consecutive pairs of frames from the same IVM are presented in Figure 4. The mean and standard deviation values of the original frames (before registration - left panel of Figure 4) were, respectively, 35.28 dB and 3.13 dB, whereas for registered frames (right panel) they were 37.79 dB and 1.62 dB, respectively. These responses show a considerable reduction in image motion despite the

TABLE II
VALUES ASSESSED FOR THE DETECTION OF THE LEUKOCYTES. THE TOTAL NUMBER OF LEUKOCYTES IN THE VIDEO IS 5851.

Methods	**Counting**			**Precision**	**Recall**	**F1-Score**	**AUCPR**
	detected leukocytes (TP)	**false alarms (FP)**	**missing leukocytes (FN)**	**TP/(TP+FP)**	**TP/(TP+FN)**	**2TP/(2TP+FP+FN)**	
Hessian-based	5010	1160	841	0.81	0.86	0.83	0.82
Template Matching	4285	720	1566	0.86	0.73	0.79	0.72

relatively small values of PSNR (less than 40dB), which is caused by an increasing in the residual image intensities due to the inherent movement of leukocytes in the images.

To assess the performance of our proposed method, centroids of the detected leukocytes were compared with those obtained by Template Matching (TM) technique [25] and with the ones manually annotated and saved in the ground-truth dataset. In this work, a leukocyte was considered correctly detected if the position of its centroid was less than 5 pixels away from the closest leukocyte in the ground-truth dataset. The distance of 5 pixels was chosen according to the average radius of the leukocytes manually annotated in the images.

The overall performance of our proposed method for the detection of leukocytes in IVM was evaluated by the classical measures precision, recall and F1-Score [26], which are commonly used in the content-based retrieval community. This technique (refer to Figure 5) plots precision (the number of leukocytes correctly detected (TP) divided by the total number of detected leukocytes (TP+FP)) versus recall (TP divided by the total number of leukocytes manually annotated (TP+FN)). FP and FN correspond, respectively, to the number of false-positive and false-negative leukocytes. Each operating point in the precision-recall plots was obtained by fixing a threshold value and comparing it with the average intensity of each region where a candidate leukocyte was detected. If the average intensity of the region is smaller than the threshold, then the candidate leukocyte is removed, otherwise it is considered for computing the precision and recall values.

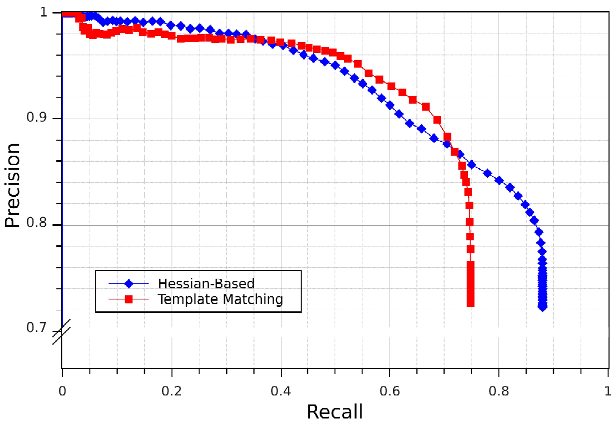

Fig. 5. Precision recall curves obtained for the proposed method (Hessian-based) and the TM.

As it can be seen in Figure 5, the proposed Hessian-based method presents a better performance than the TM if we consider the area under both precision-recall curves (AUCPR), which are 0.82 and 0.72, respectively. For recall values smaller than 0.73, the precision of both methods is very similar. However, if we consider recall values greater than 0.73, then the precision of the Hessian-based method is considerably higher than the TM.

In addition to the plots in Figure 5, we have also determined the best F1-Score values for both the Hessian and TM methods. This score, which is a measure of a test's accuracy, can also be interpreted as a harmonic mean of the precision and recall, where a F1-score reaches its best value at 1 and worst score at 0. The results, summarized in Table II, indicate that, for this specific operating point, the proposed Hessian-based method achieved better accuracy than the TM.

Our proposed method was also assessed by means of the average AUCPR measure ($\overline{\text{AUCPR}}$, computed from AUCPR measures estimated for all individual video frames) and its 95% confidence interval. In this case, the results obtained for proposed method and the TM were, respectively, 0.79 [CI: 0.78 - 0.80] and 0.68 [CI: 0.67 - 0.69].

Figure 6 depicts a resulting image of a video frame processed in this work by the Hessian-based and TM methods. The original frame is shown in Figure 6(a), while the leukocytes manually annotated can be seen as blue circles in Figure 6(b). Figures 6(c) and (d) illustrate using small green circles the detected leukocytes. White squares and blue circles indicate, respectively, the FP and FN leukocytes. In this specific image, we can notice that the Hessian-based method have correctly detected a larger number of leukocytes compared with the TM. The numbers of FP and FN are also smaller for the Hessian method.

IV. CONCLUSIONS

In this work we have presented a fully automatic method for video stabilization and detection of leukocytes in intravital video microscopy. Detecting rolling and adhered leukocytes in video sequences of *in vivo* animal brain studies is a very challenging task. The major problems are the severe image noise and clutter, the unavoidable presence of motion blur in the images, caused mainly by heart beat and respiratory movements of the animal, and the high variability in contrast between cells and background. To address these problems we have developed a video motion stabilization algorithm based on a temporal image registration technique. This approach, which involves affine and deformable transformations to correct for image motion, was qualitatively and quantitatively assessed and its results have shown a considerably improvement in IVM stabilization. To handle high variability in image

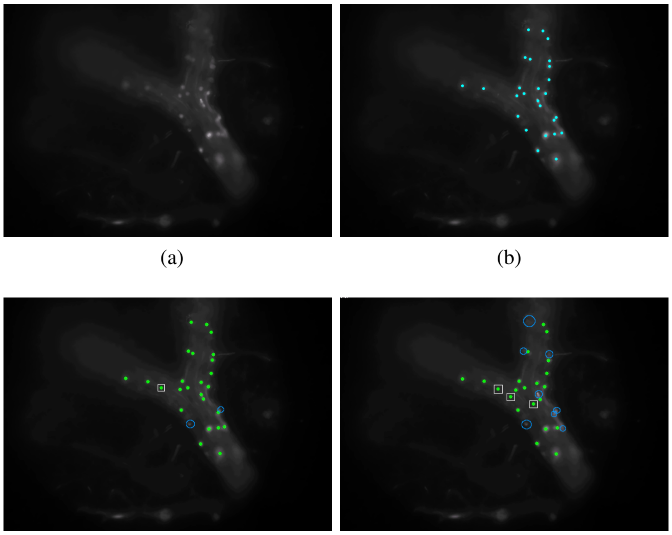

(a) (b) (c) (d)

Fig. 6. Example of a processed video frame. (a) Original frame, (b) leukocytes manually annotated - ground-truth, and (c) and (d) are, respectively, the output of the Hessian-based and TM methods. White squares in images (c) and (d) indicate the FP leukocytes, whereas the blue circles represents the FN. Leukocytes detected by both methods are shown as green circles.

contrast, we have developed a method based on analysis of Hessian matrix eigenvalues to detect leukocytes in the images. By using an IVM composed of 220 frames (with 5851 leukocytes manually annotated), the method was quantitatively evaluated (in comparison with the ground-truth) and its results have demonstrated their effectiveness for the detection of leukocytes. Besides, our proposed method has shown better performance when compared with the TM technique (AUCPR of 0.82 versus 0.72).

Acknowlegments

The authors are grateful to “Conselho Nacional de Desenvolvimento Científico e Tecnológico (CNPq)” (process number 481923/2010-1) and to grant #2012/17772-3 and #2013/26171-6, São Paulo Research Foundation (FAPESP) for their invaluable financial support during the course of this research.

References

[1] P. Kubes and S. Kerfoot, “Leukocyte recruitment in the microcirculation: the rolling paradigm revisited,” *News in Physiological Sciences*, vol. 16, no. 2, pp. 76–80, 2001.

[2] V. Pinho, F. Matos, G. Batista, and D. Carmona, *Light Microscopy - Methods in Molecular Biology*, 2011, vol. 689, ch. 6 - Intravital Microscopy to Study Leukocyte Recruitment In Vivo, pp. 81–90.

[3] Y. Sato, J. Chen, R. A. Zoroofi, N. Harada, S. Tamura, and T. Shiga, “Automatic extraction and measurement of leukocyte motion in microvessels using spatiotemporal image analysis,” *IEEE Transactions on Biomedical Engineering*, vol. 44, no. 4, pp. 225–236, 1997.

[4] S. T. Acton, K. Wethmar, and K. Ley, “Automatic tracking of rolling leukocytes in vivo,” *Microvascular Research*, vol. 63, no. 1, pp. 139–148, 2002.

[5] N. Ray, S. T. Acton, and K. Ley, “Tracking leukocytes *in vivo* with shape and size constrained active contours,” *IEEE Transactions on Medical Imaging*, vol. 21, no. 10, pp. 1222–1235, 2002.

[6] S. T. Acton and N. Ray, “Detection and tracking of rolling leukocytes from intravital microscopy,” in *Proceedings of the IEEE International Symposium on Biomedical Imaging: Nano to Macro*, vol. 2. IEEE, 2004, pp. 1235–1238.

[7] N. Ray and S. T. Acton, “Motion gradient vector flow: An external force for tracking rolling leukocytes with shape and size constrained active contours,” *IEEE Transactions on Medical Imaging*, vol. 23, no. 12, pp. 1466–1478, 2004.

[8] D. Mukherjee, N. Ray, and S. Acton, “Level set analysis for leukocytes detection and tracking,” *IEEE Transactions on Medical Imaging*, vol. 13, no. 4, pp. 562–572, 2004.

[9] G. Dong, N. Ray, and S. T. Acton, “Intravital leukocyte detection using the gradient inverse coefficient of variation,” *IEEE Transactions on Medical Imaging*, vol. 24, no. 7, pp. 910–924, 2005.

[10] G. Dong and S. T. Acton, “Detection of rolling leukocytes by marked point processes,” *Journal of Electronic Imaging*, vol. 16, no. 3, pp. 033 013:1–11, 2007.

[11] R. J. Ferrari, C. H. Villa Pinto, B. C. Gregório da Silva, D. Bernardes, and J. Carvalho-Tavares, “Automatic detection of motion blur in intravital video microscopy image sequences via directional statistics of log-gabor energy maps,” *Medical and Biological Engineering and Computing*, vol. 53, no. 2, pp. 151–163, 2015.

[12] C. Tomasi and R. Manduchi, “Bilateral filtering for gray and color images,” in *Proceedings of the Sixth International Conference on Computer Vision*, ser. ICCV’98. Bombay, India: IEEE Computer Society, 1998, pp. 839–846.

[13] V. Andresen, K. Pollok, J.-L. Rinnenthal, L. Oehme, R. Günther, H. Spiecker, H. Radbruch, J. Gerhard, A. Sporbert, Z. Cseresnyes, A. E. Hauser, and R. Niesner, “High-resolution intravital microscopy,” *PLoS ONE*, vol. 7, no. 12, pp. e50 915:1–12, 2012.

[14] L. G. Nyúl, J. K. Udupa, and X. Zhang, “New variants of a method of MRI scale standardization,” *IEEE Transactions on Medical Imaging*, vol. 19, no. 2, pp. 143–150, 2000.

[15] J. P. W. Pluim, J. B. A. Maintz, and M. A. Viergever, “Mutual-information-based registration of medical images: a survey,” *IEEE Transactions on Medical Imaging*, vol. 22, no. 8, pp. 986–1004, 2003.

[16] S. Klein, J. P. W. Pluim, and M. Staring, “Adaptive stochastic gradient descent optimisation for image registration,” *International Journal of Computer Vision*, vol. 81, no. 3, pp. 227–239, 2009.

[17] J.-P. Thirion, “Image matching as a diffusion process: An analogy with Maxwell’s demons,” *Medical Image Analysis*, vol. 2, no. 3, pp. 243–260, 1998.

[18] B. Avants, N. Tustison, and G. Song, *Advanced Normalization Tools (ANTS)*. University of Pennsylvania, 2009.

[19] B. K. P. Horn and B. G. Schunck, “Determining optical flow,” *Artificial Intelligence*, vol. 17, no. 1-3, pp. 185–203, 1981.

[20] O. P. Dzyubak and E. L. Ritman, “Automation of hessian-based tubularity measure response function in 3D biomedical images,” *International Journal of Biomedical Imaging*, vol. 2011, no. Article ID 920401, 16 pages, 2011.

[21] T. Lindeberg, “Feature detection with automatic scale selection,” *International Journal of Computer Vision*, vol. 30, no. 2, pp. 79–116, 1998.

[22] P. Majer, “The influence of the gamma-parameter on feature detection with automatic scale selection,” in *Proceedings of the Third International Conference on Scale-Space and Morphology in Computer Vision*, ser. Scale-Space 2001. Springer-Verlag, 2001, pp. 245–254.

[23] A. F. Frangi, W. J. Niessen, K. L. Vincken, and M. A. Viergever, “Multiscale vessel enhancement filtering,” in *Proceedings of the Medical Image Computing and Computer-Assisted Interventation*, vol. 1496. Cambridge, MA, USA: Springer-Verlag, pp. 130–137.

[24] A. C. dos Santos, M. M. Barsante, R. M. Arantes, C. C. Bernard, M. M. Teixeira, and J. Carvalho-Tavares, “CCL2 and CCL5 mediate leukocyte adhesion in experimental autoimmune encephalomyelitis an intravital microscopy study,” *Journal of Neuroimmunology*, vol. 162, no. 1-2, pp. 122–129, 2005.

[25] M. Khosravi and R. W. Schafer, “Template matching based on a grayscale hit-or-miss transforma,” *IEEE Transactions on Image Processing*, vol. 5, no. 6, pp. 1060–1066, 1996.

[26] C. Goutte and E. Gaussier, “A probabilistic interpretation of precision, recall and f-score, with implication for evaluation,” in *Proceedings of the European Colloquium on IR Research*, ser. ECIR’05. Springer, 2005, pp. 345–359.